ADAPTIVE FINITE ELEMENT METHODS FOR FLUORESCENCE ENHANCED FREQUENCY DOMAIN OPTICAL TOMOGRAPHY: FORWARD IMAGING PROBLEM

Amit Joshi[1], Wolfgang Bangerth[2], Alan B. Thompson[1] and Eva M. Sevick-Muraca[1]
[1] Photon Migration Laboratories, Texas A& M University, College Station, TX
[2] Center for Subsurface Modeling, ICES, University of Texas at Austin, TX

ABSTRACT

In this contribution we introduce adaptive finite element methods for forward modeling in fluorescence optical tomography. Adaptive local mesh refinement increases the accuracy of the solutions of coupled photon diffusion equations in a computationally optimal manner and when implemented in the inverse problem, can impact the resolution of fluorescence enhanced tomography. An adaptive Galerkin finite element scheme is implemented and the simulation results are compared with experimental data obtained from a tissue phantom by an area illumination and area detection scheme.

1.0 INTRODUCTION

Fluorescence enhanced frequency domain optical tomography is an emerging functional imaging modality which involves the administration of a fluorescent contrast agent as opposed to radio-isotope as is used in conventional nuclear imaging techniques. NIR fluorescence enhanced imaging may be sensitive to targets with nano-molar concentrations of fluorophore making it ideal for molecular imaging applications [1]. Fluorescence enhanced optical tomography can provide images of fluorescent yield and lifetime within the tissue domain by utilizing the boundary measurements of photon energy resulting from the tissue stimulation via infrared light sources at the boundary. Tomography requires repeated solution of a system of coupled elliptic partial differential equations describing the time-dependent fluorescent light generation and transport within the tissue.

The finite element solver for the system of equations constitutes the bulk of computational cost of tomographic imaging. Since near infrared light attenuates rapidly in tissue, the light energy distribution within the tissue has steep gradients. To accurately predict energy distributions, the finite element mesh needs to be suitably refined near the light sources and boundaries. Traditionally this task has been performed *a priori* with meshes optimally designed for given imaging geometries. In this contribution we propose the use of *a posteriori* error estimates for adaptive mesh refinement to optimally model the strongly graded light distribution within tissues. Specifically we demonstrate this novel forward modeling scheme for fluorescence frequency domain measurements performed by the innovative use of area illumination and area detection on the surface of a tissue phantom [2, 3]

2.0 BACKGROUND

In frequency-domain fluorescence optical tomography, the propagation of intensity modulated near infrared excitation light and the generation and propagation of emitted fluorescent light is described by the coupled diffusion equations:

$$-\nabla\bullet[D_x(\mathbf{r})\nabla\Phi_x(\mathbf{r},\omega)]+k_x\Phi_x(\mathbf{r},\omega)=0 \qquad (1)$$

$$-\nabla\bullet[D_m(\mathbf{r})\nabla\Phi_m(\mathbf{r},\omega)]+k_m\Phi_m(\mathbf{r},\omega)=\beta_{xm}\Phi_x(\mathbf{r},\omega) \qquad (2)$$

$$k_x=\frac{i\omega}{c}+\mu_{axi}(\mathbf{r})+\mu_{axf}(\mathbf{r})$$

$$k_m=\frac{i\omega}{c}+\mu_{ami}(\mathbf{r})+\mu_{amf}(\mathbf{r})$$

$$\beta_{xm}=\frac{\phi(\mathbf{r})\mu_{axf}(\mathbf{r})}{1-i\omega\tau(\mathbf{r})}$$

Where $\Phi_{x,m}$ (photons/cm^{2}s) is the complex photon fluence of the excitation (subscript x) or emission (subscript m); $D_{x,m}$ (cm) is the optical diffusion coefficient at the excitation or emission wavelength; c is the velocity of light in the media; $\mu_{ax,mi}$ (cm^{-1}) is the absorption owing to the non fluorescing chromophores; $\mu_{ax,mf}$ (cm^{-1}) is the absorption due to exogenous fluorophores; ω is the angular modulation frequency (rad/s); ϕ is the quantum efficiency of the fluorescent emission and τ is the lifetime(ns) of the fluorophores. Equations (1) and (2) are solved with the Robin boundary conditions:

$$2\gamma D_{x,m}\frac{\partial\Phi_{x,m}(\mathbf{r},\omega)}{\partial n}+\Phi_{x,m}(\mathbf{r},\omega)+S_x(\mathbf{r})=0 \qquad (3)$$

Where n denotes the outward normal to the surface; γ is a constant accounting for the refractive index mismatch at the boundary; $S_x(\mathbf{r})$ term appears in

the boundary condition for equation (1) only and it accounts for the excitation source distribution.

The forward imaging problem for fluorescence enhanced optical tomography constitutes the determination of boundary emission fluence for a given optical property distribution in the tissue domain.

3.0 FINITE ELEMENT SOLUTION SCHEME

We have employed the Galerkin finite element method for solving Equations (1) and (2). The weak or variational form of eqns (1) and (2) with boundary conditions provided by eqn (3) can be written as:

$$a_x(\Phi_x, w) = (f_x, w)$$
$$a_m(\Phi_m, w) = (f_m, w) \quad (4)$$

Where $a_{x,m}(\Phi_{x,m}, w)$ are the bilinear forms associated with the coupled diffusion equations and $(f_{x,m}, w)$ are the linear forms for the right hand side; w denotes the weighting functions. The solution of the variational problem $[\Phi_x, \Phi_m] \in V$ satisfies the system of equations (4) for all $w \in V$; V is the vector space of approximating functions. For the finite element method V is the space of piecewise polynomials. Although triangular and tetrahedral elements are popular in the optical tomography community, we have chosen eight node tri-linear hexahedral brick shaped elements since they allow efficient and computationally stable implementation of adaptive mesh refinement.

The excitation and emission fluences are approximated as:

$$\Phi_{x,m} = \sum_{n=1}^{8} \Phi_{x,m}^{n} w_n \quad (5)$$

Here $\{w_1, w_2, w_3 \ldots\ldots\ldots w_n\}$ are the nodal basis functions for the finite element space V and $\Phi_{x,m}^{n}$ denotes the fluence values at the nth node. With these substitutions, the system of equations (4) is transformed into a linear system of equations for each element which are then assembled into a global linear system. The unknowns of the global linear system are the nodal values of excitation and emission fluences:

$$K_x \overline{\Phi}_x = b_x$$
$$K_m \overline{\Phi}_m = B_{xm} \overline{\Phi}_x \quad (6)$$
$$\overline{\Phi}_{x,m} = transpose[\Phi_{x,m}^{1}, \Phi_{x,m}^{2}, \Phi_{x,m}^{3} \ldots\ldots\ldots \Phi_{x,m}^{N}]$$

$K_{x,m}$ are the global stiffness matrices resulting from the L.H.S integrals in equations (4); b_x is the source vector for the excitation equation; B_{xm} is the coupling matrix resulting from the R.H.S of the emission diffusion equation. The number of unknowns in this system is on the order of 10^4 for fluorescence tomography applications in large tissue mimicking phantoms. Clearly optimal mesh generation is essential for accurate solution at a reasonable computational cost.

3.1 *A posteriori error estimation and adaptive mesh generation*

The error in finite element solution scales with the element size. Hence the accuracy of the solution increases with mesh refinement. With only a-priori knowledge of the error in finite element solution, uniform global mesh refinement is the only possible means to improve the accuracy of the solution, However in fluorescence tomography applications where solutions have large gradients within only limited regions of the domain, global mesh refinement can result in millions of nodes, which makes the solution for the system of equations (6) computationally impractical. Local mesh refinement within the regions associated with large variation of the excitation or emission fluence increases the accuracy of the solutions while keeping the degrees of freedom of the system in check. In this work the solution process is started with a coarse mesh and successive meshes are generated according to an a-posteriori error estimator. We have used the error estimator developed by Kelly [4]. Kelly's error estimator is a residual based energy norm estimator which refines the mesh, at locations where the gradient of the solution shows rapid spatial variation. After the solution on the coarse mesh, the error for each element is calculated by the following equation:

$$\varepsilon_K = \frac{h}{24} \left\| [\partial_n \Phi_{x,m}] \right\|_{\partial K}^{2} \quad (7)$$

Where ε_K is the error for Kth finite element; h is the element size measure; $[\partial_n \Phi_{x,m}]$ is the jump of normal derivative of the finite element solution across the element boundary ∂K. For our implementation we refine 70% of the elements with highest error values and coarsen 3% of the elements with lowest errors in each cycle. Some other elements are also refined to a lower degree to maintain numerical stability of the solution.

The entire scheme for the solution of coupled diffusion equations with adaptive mesh refinement was programmed in C++ utilizing Deal.II finite element

libraries. Deal.II was developed by a team of developers led by Dr. Wolfgang Bangerth [5]. Deal.II provides advanced object oriented design techniques and support for complex data structures needed for adaptive finite element applications.

4.0 FORWARD MODELING FOR AREA ILLUMINATION AND AREA DETECTION SCHEMES

The adaptive forward solver was used to predict the fluorescent frequency domain photon migration measurements from a tissue phantom containing a fluorescent target, by means of area illumination and area detection on the same surface. The phantom was an 8x8x8 cm^3 container filled with 1% Liposyn solution with a 1-ml "target" containing 1-micromolar concentration of Indocyanine Green in 1% Liposyn suspended within the phantom at a depth of 1 cm from the surface. The tissue phantom was illuminated with an expanded laser beam of 785 nm excitation light. The excitation light was intensity modulated at 100 MHz. Area detection of frequency-domain parameters of amplitude and phase shift accomplished using a gain modulated image intensified charge coupled device. The experimental setup employed is detailed in Figure-1 [2]. The reader is referred to references [1] and [2] for the details of instrumentation and data acquisition scheme.

The finite element simulation was started with a uniform coarse mesh with the discretization level of 16 x 16 x 16 elements. Three adaptive local mesh refinements were carried out to obtain a resolution of 0.0625 x 0.0625 cm at the detection surface which matched the measurement resolution of the image captured by the CCD. The simulated values of amplitude and phase shift for fluorescence were referenced with respect to the point on surface with maximum fluorescent amplitude and the referenced simulated and experimental measurements were compared to analyze the model match.

5.0 RESULTS AND DISCUSSIONS

Figure-2 depicts the evolution of mesh with the three adaptive local refinements on a cut plane drawn at $x = 4$. The final mesh contained 147292 nodes. The total computer time taken for solution was 15 minutes on a dual processor Sun Sparc workstation. The mesh is refined in the regions with large gradients in the excitation and emission fields. Figures 3 and 4 show the fluorescent amplitude and phase on the detection area on the top surface for the experimentally measurements and the finite element simulation. The average error between the measurement and prediction using the adaptive finite element predictor is 12.25% for fluorescent amplitude and 1.47° for fluorescent phase. The highest errors are observed at the edges of the detection area and are attributed to edge effects in the ICCD detection system.

6.0 CONCLUSIONS

We have demonstrated a novel approach for finite element based forward modeling in fluorescence enhanced optical tomography. With adaptive local refinement there is no need for suitable *a priori* designed finite element meshes for accurate solution of diffusion equations. The solutions from adaptive finite element solver match the experimentally observed fluorescent field within reasonable limits of experimental error. Currently work is under progress for the application of adaptive mesh refinement techniques for the inverse problem of estimating the fluorescent yield distribution in the tissue domain by using an adaptive discretization of the unknown fluorescent yield.

7.0 REFERENCES

[1] Houston, J.P., Thompson, A.B., Gurfinkel, M., and E.M. Sevick-Muraca, *Sensitivity and penetration depth of NIR fluorescence contrast enhanced diagnostic imaging,* Photochem. Photobiol., 77: 2003. Erratum, 77(4): 103, 2003.

[2] Thompson, A.B., Hawyrsz, D.J., and **E.M. Sevick-Muraca,** "*Near-infrared fluorescence contrast enhanced imaging with area illumination and area detection: the forward imaging problem*," Applied Optics, 42(19), 4125-4136, 2003.

[3] R. Roy*, A. B. Thompson, A. Godavarty, E. M. Sevick-Muraca, "*Tomographic fluorescence imaging in tissue phantoms: a novel reconstruction algorithm and imaging geometry,"* submitted to IEEE Trans. Med. Imaging.

[4] D.W Kelly et al, "*A posteriori error estimates and adaptive processes in the finite element method: part(1) error analysis*," Int. J. Num. Meth. Engg. **19** (1983).

[5] Wolfgang Bangerth and Guido Kanschat, "*Concepts for object oriented finite element software- the deal.II library*," Preprint 99-43 (SFB 359), IWR Heidelberg, (1999)

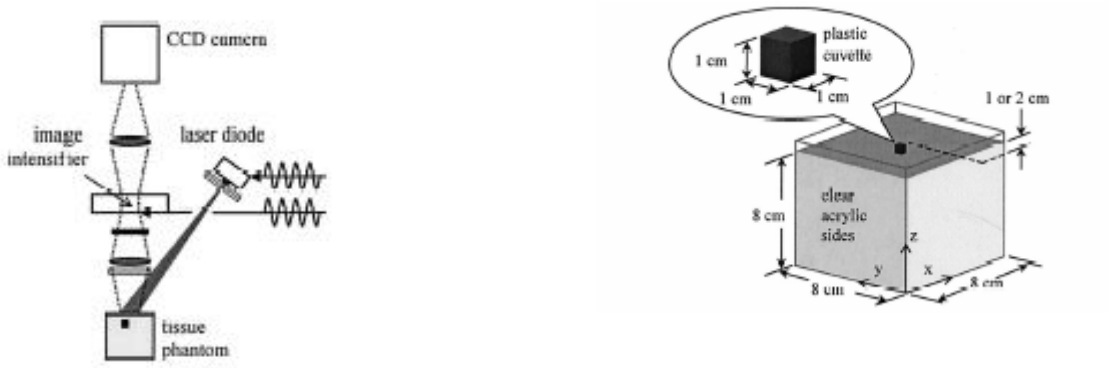

Figure-1: Instrumentation Details [2]

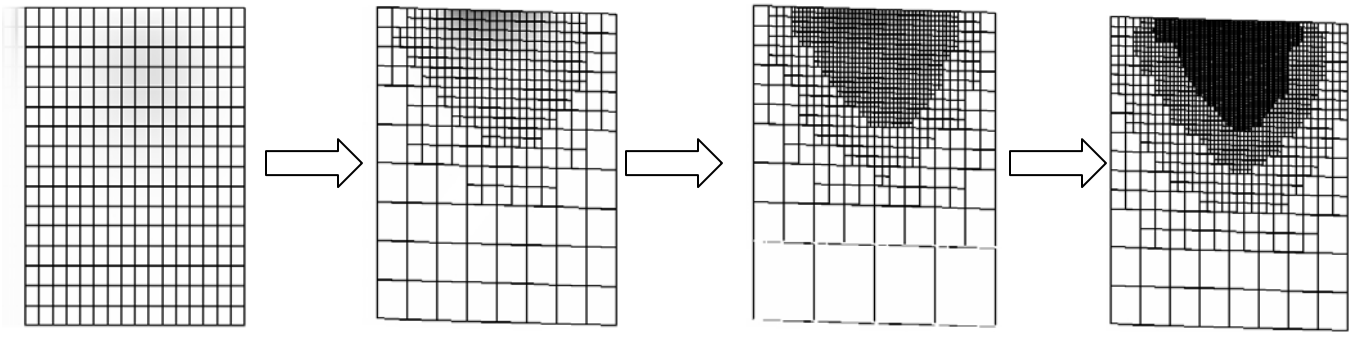

Figure-2: Evolution from initial coarse mesh to locally refined mesh in three steps Meshes at Cutting planes drawn at x = 4 are depicted

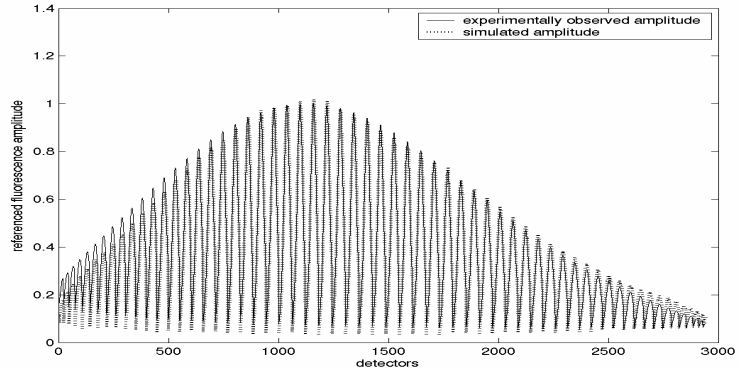

Figure-3: Model match for experimentally observed fluorescent amplitude(referenced)

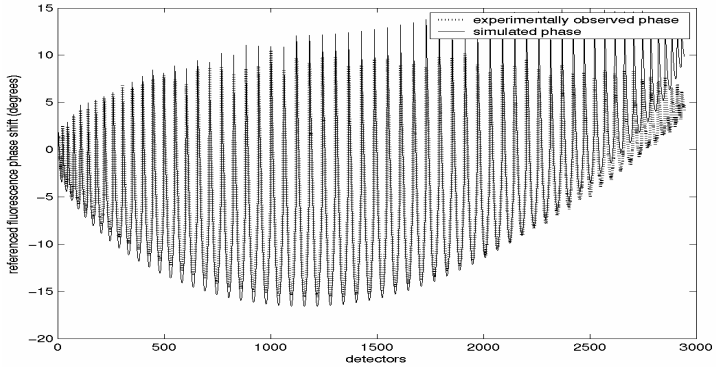

Figure-4: Model match for experimentally observed fluorescent phase (referenced)